

1 Performance evaluation of MOMA - a remote network calibration 2 technique for PM_{2.5} and PM₁₀ sensors

3 Lena Francesca Weissert¹⁾, Geoff Steven Henshaw¹⁾, David Edward Williams²⁾, Brandon Feenstra³⁾,
4 Randy Lam³⁾, Ashley Collier-Oxandale³⁾, Vasileios Papapostolou³⁾ and Andrea Polidori³⁾

5
6 ¹Aeroqual Ltd, 460 Rosebank Road, Avondale, Auckland, 1026, New Zealand

7 ²School of Chemical Sciences and MacDiramid Institute for Advanced Materials and Nanotechnology, University of
8 Auckland, Private Bag 92019, Auckland, 1142, New Zealand

9 ³South Coast Air Quality Management District, 21865 Copley Drive, Diamond Bar, CA, 91765, USA

10

11

12 *Correspondence to:* Lena Weissert (lena.weissert@aeroqual.com)

13

14 **Abstract.** We evaluate the potential of using a previously developed remote calibration framework we name MOMA (MOment
15 MAtching) to improve the data quality in PM sensors deployed in hierarchical networks. MOMA assumes that a network of
16 reference instruments can be used as ‘proxies’ to calibrate the sensors given that the probability distribution over time of the
17 data at the proxy site is similar to that at a sensor site. We use the reference network to test the suitability of proxies selected
18 based on distance versus proxies selected based on land use similarity. The performance of MOMA for PM sensors is tested
19 with sensors co-located with reference instruments across three Southern California regions, representing a range of land uses,
20 topography, and meteorology, and calibrated against a distant proxy reference. We compare two calibration approaches, one
21 where calibration parameters get calculated and applied at monthly intervals and one which uses a drift detection framework
22 for calibration. We demonstrate that MOMA improves the accuracy of the data when compared against the co-located reference
23 data. The improvement was more visible for PM₁₀ and when using the drift detection approach. We also highlight that sensor
24 drift was associated with variations in particle composition rather than instrumental factors explaining the better performance
25 of the drift detection approach if wind conditions and associated PM sources varied within a month.

26

27 1 Introduction

28 Particulate matter (PM) is a major air pollutant with negative impacts on both the environment and human health (Kim et al.,
29 2015; Anderson et al., 2012; Pope Iii, 2002; Rai, 2016). Smaller particles, known as PM_{2.5} (particles with an aerodynamic
30 diameter < 2.5µm) have the ability to penetrate deep into the lung and to cross into the blood stream, and trigger inflammatory
31 and mutagenic responses linked amongst other effects to cardio-pulmonary disorders, diabetes and adverse birth outcomes
32 (Feng et al., 2016). Coarse PM (PM_{10-2.5}) tend to impact the upper respiratory tract and induce respiratory symptoms such as
33 cough (Pope and Dockery, 1992). Short-term exposures to PM₁₀ have been associated primarily with worsening of respiratory
34 diseases, including asthma and chronic obstructive pulmonary disease (COPD) (California Air Resources Board, 2023). The

35 spatial and temporal variability of PM is driven by multiple factors including anthropogenic emissions PM from traffic,
36 construction, and residential heating which are main contributors to PM_{2.5} as well as natural sources such as mineral dust
37 consisting mainly of particles in the coarse fraction (PM_{10-2.5}) (Anderson et al., 2012; Atkinson et al., 2010). PM_{2.5} and PM₁₀
38 are routinely measured by government and research organisations using reference-grade equipment that is either filter-based
39 Federal Reference Method (FRM) or continuous Federal Equivalence Method (FEM). However, reference monitoring
40 networks are designed to measure regional air pollution to determine attainment of national ambient air quality standards and
41 are often sparsely sited across a region due to high instrument and operational costs (Morawska et al., 2018; Snyder et al.,
42 2013). The last decade has seen a rapid increase in the availability of PM sensors offering opportunities to measure PM with
43 much denser networks and making them popular choices for citizen projects and community monitoring (Giordano et al., 2021;
44 Liang, 2021; Snyder et al., 2013; Zimmerman, 2022).

45 Most PM sensors are optical sensors that utilize the light scattered by particles to determine the particle size and count which
46 are then converted to particle mass based on assumptions about particle density, shape and refractive index. This poses a major
47 challenge for calibrating PM sensors as calibration factors may change with particulate type and composition as well as
48 meteorological conditions such as temperature or relative humidity (RH) which cause the particles to swell or shrink and
49 change their light scattering (Badura et al., 2018; Morawska et al., 2018; Ouimette et al., 2022).

50 Thus, frequent field calibrations may be required if aerosol properties vary significantly over time (Liang, 2021; Johnson et
51 al., 2018; Badura et al., 2018). While calibrations by co-location using regression analysis remain a popular choice the costs
52 and feasibility related to individual site visits and calibrations make them not a viable option for large and/or long-term sensor
53 networks (Liang, 2021). Another approach is to apply a RH correction factor to account for the bias introduced due to high
54 RH (Crilley et al., 2020; Liang, 2021). While this method has the advantage of being independent from the availability of
55 reference data it is not suitable for locations with consistently high RH and does not improve the accuracy as much as other
56 calibration methods (Liang, 2021). Similarly, Barkjohn et al. (2021) developed a US nation-wide correction for PurpleAir
57 Sensors which is implemented in the Airnow Fire and Smoke Map (<https://fire.airnow.gov/>). While the approach has
58 intensively been tested for PurpleAir sensors, further research is required to evaluate its transferability to other sensor models
59 (Barkjohn et al., 2021). Other studies have used Machine learning (ML) approaches to train calibration models with enough
60 co-location data to cover various meteorological and environmental conditions and make them more robust for long-term
61 sensor deployments (Liang, 2021; De Vito et al., 2020; Loh and Choi, 2019). However, if conditions (e.g., different traffic
62 conditions, different PM sources) at the co-location site are different from the conditions at the site of the final deployment the
63 model may no longer be suitable (De Vito et al., 2020; Liang, 2021). In addition, while being more robust and effective, ML
64 may still suffer from challenges related to sensor degradation when sensors are deployed in a long-term fashion (Liang, 2021).

65 In previous publications, we demonstrated that a hierarchical network, consisting of well-maintained reference-grade
66 instruments (referred to as ‘proxies’) and gas-phase (O₃, NO₂) sensors can be used to correct sensors remotely (Miskell et al.,

67 2018, 2019; Weissert et al., 2020). The correction framework, that we named MOMA for MOment MAtching, is based on the
68 assumption that the probability distribution over time of measurements at a proxy site is similar to that of the sensor site
69 (Miskell et al., 2018, 2019; Weissert et al., 2020). We have demonstrated that this approach is able to successfully correct for
70 sensor drift without the need of co-location.

71 In this paper, we examine how this remote calibration methodology performs for PM sensors deployed in Southern California.
72 The network was established between 2020 and 2022 to supplement the reference network and supports California Assembly
73 Bill 617 community monitoring. The network is maintained by South Coast AQMD and covers three main regions, including
74 the City of Los Angeles (LA), the Inland Empire (IE), and a desert region of Riverside County (RC Desert). These three regions
75 differ in terms of land use, terrain and meteorology offering an opportunity to test MOMA under different seasonal conditions
76 and PM sources.

77 The network consists of over 60 sensors, for which the overhead for manual calibration would be prohibitive. Thus, using the
78 MOMA approach, the sensors are calibrated at monthly intervals and new calibration gains and offsets are uploaded to a cloud
79 to provide real-time calibrated data which is displayed on the South Coast AQMD AQPortal (<https://aqportal.aqmd.gov/>). In
80 order to validate the MOMA procedure applied across the network, the focus of this paper is on six sensors that are co-located
81 with a reference instrument at Air Monitoring Sites (AMS). Here, we compare the monthly calibration approach to an
82 automated drift detection approach to apply the calibration when drift between a sensor and the proxy site was detected using
83 data from January to December 2021 (Miskell et al., 2018, 2019; Weissert et al., 2020).

84 A key part of MOMA is the identification of a suitable proxy site for each sensor in the sensor network. Previous work has
85 shown that the nearest reference site is a suitable proxy to calibrate O₃ concentrations, which are regionally well correlated
86 (Miskell et al., 2018, 2019). For NO₂, which is spatially and temporally more variable, land use similarity proved to be good
87 criteria to select appropriate proxy sites (Weissert et al., 2020). PM_{2.5} levels tend to be relatively homogeneous across an urban
88 region suggesting that the closest reference site could be a suitable proxy. However, PM₁₀ can be spatially more variable due
89 to the shorter lifetime and more variable sources, and a proxy selected based on distance may not be suitable (Pinto et al.,
90 2004; Sardar, 2005). Thus, we also determine suitable proxies for calibrating PM_{2.5} and PM₁₀.

91 2 Materials and Methods

92 2.1 Data

93 This study uses data from a network of AQY v1.0 (AQY) sensor systems from Aeroqual Ltd, Auckland, New Zealand. The
94 AQY measures O₃, NO₂, PM_{2.5}, PM₁₀, Temperature, and Relative Humidity. Detailed description about the AQY sensor system
95 is available in Weissert et al. (2020) and Miskell et al. (2019). The focus of this paper is the PM sensor (model SDS011, Nova
96 Fitness Co., Ltd, Jinan City/China) inside the AQY sensor system. The SDS011 is an optical light scattering device which
97 outputs PM_{2.5} and PM₁₀ mass concentration ($\mu\text{g m}^{-3}$) measurements. Previous studies of this sensor have shown high PM_{2.5}

98 correlation with reference instruments (Badura et al., 2018; Liu et al., 2019) but PM₁₀ values may be underestimated (Budde
 99 et al., 2018; Kuula et al., 2020). Nevertheless, we use both PM_{2.5} and PM₁₀ measurements to evaluate the performance of our
 100 network calibration technique applied to PM data. The SDS011 sensor was factory calibrated against a Met One 9722 8 channel
 101 optical particle counter (Met One Instruments, Inc., Grants Pass, Oregon, US) using 1 µm latex microspheres. The AQY
 102 performs a humidity correction using an algorithm based on the κ-Köhler theory with an empirically derived scalar (Crilley et
 103 al., 2018). The AQY PM measurements were field and laboratory evaluated by South Coast AQMD's Air Quality Sensor
 104 Performance Evaluation Centre (AQ-SPEC) (<http://www.aqmd.gov/aq-spec/sensordetail/aeroqual-aqy-v1.0>) showing strong
 105 correlations with the co-located FEM GRIMM data ($0.77 < R^2 < 0.85$) and low to moderate intra-model variability.

106
 107 We used data from six AQYs co-located at AMS sites, referred to as 'co-location sites' in this paper, equipped with a reference-
 108 grade instrument., which allowed us to test the performance of the remote calibration framework (Table 1). Reference data
 109 from the co-location AMS were obtained either from AirNow (<https://www.airnow.gov/>) or directly from South Coast AQMD.
 110 Refer to Table S1 for instrumentation at each site. The six AQYs were deployed between April 2020 and January 2021 (Table
 111 1). While PM_{2.5} data were available since the start of the deployment, PM₁₀ sensors were only activated at the start of January
 112 thus we focus on data from January to December 2021 for the following analysis. Fog can frequently be present between
 113 October and February in the study area, driven by lower inversion levels (Qin et al., 2012; Witiw and LaDochy, 2008) and
 114 lead to overestimates in PM_{2.5} and PM₁₀ (Budde et al., 2018) (Fig. S1). We developed a fog alert and data impacted by fog
 115 were removed for this analysis. This affected around 1% of the data at each site and was mostly observed in November,
 116 December and February.

117
 118 To get a better understanding about the composition of measured particles and how this impacts the performance of MOMA
 119 we used speciation data collected at the Riverside-Rubidoux (RIVR) AMS. All speciation data were obtained using the
 120 RAQSAPI package (Mccrowey et al., 2022), which enables downloading monitoring data from the US Environmental
 121 Protection Agency's Air Quality System service. We focused on parameters representing crustal material, trace ions, secondary
 122 ions, elemental carbon (EC) and organic carbon (OC) and followed the classification described in Daher et al. (2013) (Table
 123 S2).

124
 125 Surface meteorological data from Riverside Municipal airport, situated ~ 6km south of the Riverside-Rubidoux AMS, were
 126 downloaded from the NOAA Integrated Surface Database (ISD) via the worldmet Package in R (Carslaw, 2022).

127
 128 **Table 1. Information about AQY sensors and their co-location sites as well as deployment dates and data completeness**
 129 **(excluding fog data).**

AQY ID	AQY Label	Co-located AMS	Region	Deployment date	Data completeness
--------	-----------	----------------	--------	-----------------	-------------------

				(mm/dd/yyyy)	(Jan - Dec 2021)
AQY BD-1146	RIVR coloc	Riverside-Rubidoux (RIVR)	IE	4/03/2020	85%
AQY BD-1129	MLVB coloc	Mira Loma - Van Buren (MLVB)	IE	4/03/2020	86%
AQY BD-1110	CMPT coloc	Compton (CMPT)	LA	1/08/2021	71%
AQY BD-1069	CELA coloc	Los Angeles - N. Main Street (CELA)	LA	6/19/2020	98%
AQY BD-1071	INDIO coloc	Indio-29 Palms (INDIO)	RC Desert	11/03/2020	82%
AQY BD-1081	PALM coloc	Palm Springs (PALM)	RC Desert	1/08/2021	91%

130

131 The statistical analysis was performed in R (v.4.1.3) using tidyverse (Wickham and RStudio, 2022), lubridate (Spinu et al.,
132 2022), zoo (Zeileis et al., 2022), ggrepel (Slowikowski et al., 2022), openair (Carslaw and Ropkins, 2022), RAQSAPI
133 (Mccrowey et al., 2022), ggplot2 (Wickham et al., 2022b), dplyr (Wickham et al., 2022a), ggmap (Kahle and Wickham, 2013)
134 and ggpmisc (Aphalo et al., 2022).

135

136 2.2 Study area

137 This study was performed in Southern California in a region that is under the jurisdiction of the South Coast Air Quality
138 Management District (South Coast AQMD). AQY sensors measuring PM were co-located at two AMS in the City of LA
139 (CELA, CMPT), two AMS in the IE (RIVR, MLVB), and two AMS in the RC Desert (INDIO, PALM) (Table 1). The LA
140 region is representative of downtown LA and PM levels are likely dominated by emissions from transport and other combustion
141 processes (Oroumiyeh et al., 2022). The IE is situated in a predominantly rural and agricultural area about 80 km inland from
142 downtown LA. It is situated downwind from LA for the majority of the year, which means that PM levels in the area will be
143 influenced by the particulate matter coming from LA (Daher et al., 2013). North-easterly Santa Ana Winds (SAW) become
144 more frequent during the fall and winter months impacting PM levels in the IE. SAW are associated with very dry air and good
145 visibility in the absence of wildfires as urban pollutants are blown offshore. However, they are also key drivers of large
146 wildfires enabling them to spread faster and transporting smoke PM from inland areas to the more populated regions (Aguilera
147 et al., 2020). The RC Desert region is located north of Salton Sea and surrounded by mountains. The region is drier and hotter
148 compared to LA and the IE. The RC Desert experiences high levels of PM₁₀, dominated by the coarse fraction, driven by
149 erosion and increasing emissions from the drying Salton Sea (Ostro et al., 2000; Miao et al., 2022)

150

151 2.3 Remote Network Calibration

152 MOMA was developed for hierarchical air monitoring networks that consist of well-calibrated reference grade instruments
153 acting as “proxies” which are used to calibrate the sensors deployed in the field. The technique is described in detail in Miskell
154 et al. (2016, 2018, 2019). Here, we calibrated sensors co-located at the AMS against a remote reference proxy. The performance
155 of the calibration against the proxy was then evaluated by comparing the calibrated data against the co-located reference data

156 using the metrics Mean Absolute Error (MAE), Root Mean Squared Error (RMSE) and coefficient of determination (R^2). We
 157 tested two approaches to calibrate the PM_{2.5} and PM₁₀ sensors in this study.
 158 The first approach was a monthly MOMA calibration using the last two weeks of each month to select a consecutive seven-
 159 day calibration window to calculate the calibration parameters which were then applied from the first to the last calendar day
 160 of the subsequent month. The last two weeks of the month were selected to ensure most recent data were used to determine
 161 calibration gains and offsets. The calibration gains, \hat{a}_1 , and offsets, \hat{a}_0 , were calculated by matching the mean, $E\{\}$, and
 162 variance, $var\{\}$, of the sensor data, Y , at location i , and proxy data, Z , at location k over the time interval $t - t_d : t$ as described
 163 in Miskell et al. (2018, 2019) and summarised in eq. 1 and 2:

$$165 \quad \hat{a}_1 = \sqrt{\frac{var\{Z_{k,t-t_d:t}\}}{var\{Y_{i,t-t_d:t}\}}} \quad (1)$$

$$166 \quad \hat{a}_0 = E\{Z_{k,t-t_d:t}\} - \hat{a}_1 E\{Y_{i,t-t_d:t}\} \quad (2)$$

167
 168 A calibration window was considered suitable if the data completeness for both proxy and sensor was greater than 85% and
 169 the temporal variation of the sensor and proxy reference data was similar (ie there was no evidence of local effects that were
 170 only present at the sensor site or proxy site). We also avoided periods when we detected fog using Aeroqual's fog detection
 171 algorithm.

172 The second approach used a previously described drift detection framework (Miskell et al., 2016) to trigger a MOMA
 173 calibration. The drift detection framework uses three statistical tests to detect sensor drift, a two-sample Kolmogorov-Smirnov
 174 (K-S) test (K-S test: p-value), the Mean-Variance (MV) moment-matching test for the slope, \hat{a}_1 and the intercept, \hat{a}_0 . The
 175 statistical tests were calculated over a 3-day running averaging-window, t_a , and an alarm was triggered when any of the tests
 176 exceeded the predetermined threshold, t_f , for a period of consecutive 5 days. These periods were selected to limit short-term
 177 fluctuations due to local effects but to capture the regional effects, that is, to ensure that diurnal and regional variations
 178 dominate (Miskell et al. 2018, 2019). The following thresholds were used to determine if a sensor drifted: K-S test p-value <
 179 0.05 (the two distributions are significantly different); $0.75 > \hat{a}_1 > 1.25$; $-5 \mu\text{g m}^{-3} > \hat{a}_0 > 5 \mu\text{g m}^{-3}$. These thresholds may be
 180 adjusted to be more or less sensitive to differences between the sensor and the proxy data. While adjusting all parameters and
 181 alarm triggers exceeded the scope of this study preliminary analysis using data from 'RIVR coloc', 'MLVB coloc' and 'CELA
 182 coloc' showed that a shorter 4-day window, t_f , may be more suitable for the AQYs located in the IE but not the City of LA.
 183 This framework was applied to the six AQYs co-located at the AMS (Table 1) using data from January to December 2021.

184 185 2.4 Proxy selection

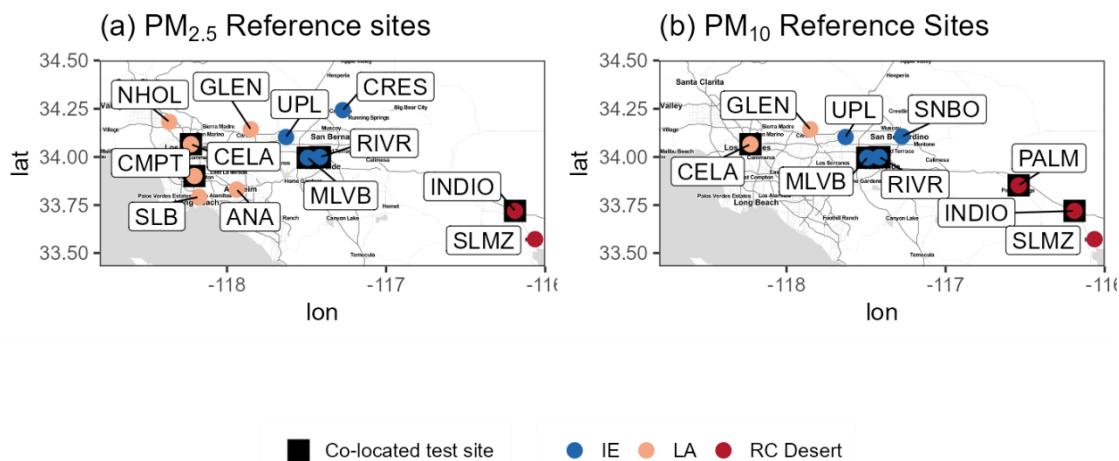
186 We compare proxies selected based on distance to proxies with similar land use. Land use variables used for the analysis were
 187 a) road length (motorway, primary roads) within a 1 km buffer around the site, b) distance of the site from a motorway and c)
 188 elevation. These are simple and widely available variables and have also been identified as good predictors for PM in land use

189 regression studies in the US (Kloog et al., 2012; Lee et al., 2016) and Europe (Eeftens et al., 2012). To select proxy sites with
 190 most similar land use we used the supervised classification technique, *k*-Nearest Neighbour classification (*k*NN) as described
 191 in more detail in Weissert et al. (2020).

192 Data from the reference network were used to identify suitable proxies, which had two main advantages over using sensor
 193 data. First, the availability of long-term reference data allowed testing and developing suitable criteria for proxy selection
 194 without relying on sensor data, which are often not available until deployed in the field. Second, we eliminated any
 195 uncertainties associated with sensor performance, such as sensor drift.

196 Figure 1 shows the network of reference PM_{2.5} and PM₁₀ monitors managed by SCAQMD. Sites with co-located AQYs,
 197 including Los Angeles, N. Main Street (CELA), Compton (CMPT), Mira Loma – Van Buren (MLVB) and Rubidoux (RIVR)
 198 were used as test locations for which a suitable PM_{2.5} proxy is found. As SLMZ was the only available PM_{2.5} proxy site for
 199 Indio-29 Palms (INDIO) this site was not included in the proxy selection analysis for PM_{2.5}. CELA, MLVB, RIVR, Palm
 200 Springs (PALM) and INDIO were used as test locations to identify suitable for PM₁₀ proxies (Fig. 1).

201 To evaluate the similarity between data at a proxy site and data at a test location we calculated the MAE, *R*², and the two-
 202 sample K-S test statistic for each possible proxy and co-located test location based on daily averaged reference data. The K-S
 203 test statistic is a measure of the maximum distance between two cumulative distributions and was used to compare the
 204 cumulative distribution of the proxy reference data to that of the reference at the co-located test location. An ideal proxy should
 205 exhibit a low MAE and K-S test statistic, as well as a high *R*² value.



206

207 **Figure 1:** a) PM_{2.5} and b) PM₁₀ South Coast AQMD reference Air Monitoring Network coloured by different regions. The map was
 208 created using ggmap (Kahle and Wickham, 2013). Co-location sites are highlighted by black squares.

209

210 **Table 2.** Table of the site names associated with the AMS IDs used in Fig. 1.

AMS ID	Name	Region
MLVB	Mira Loma - Van Buren	IE
RIVR	Riverside - Rubidoux	IE
SNBO	San Bernadino	IE
CRES	Crestline - Lake Gregory	IE
UPL	Upland	IE
CELA	Los Angeles - N. Main Street	LA
CMPT	Compton	LA
NHOL	North Hollywood	LA
ANA	Anaheim	LA
SLB	South Long Beach	LA
GLEN	Glendora - Laurel	LA
PALM	Palm Springs	RC Desert
INDIO	Indio-29 Palms	RC Desert
SLMZ	Saul Martinez	RC Desert

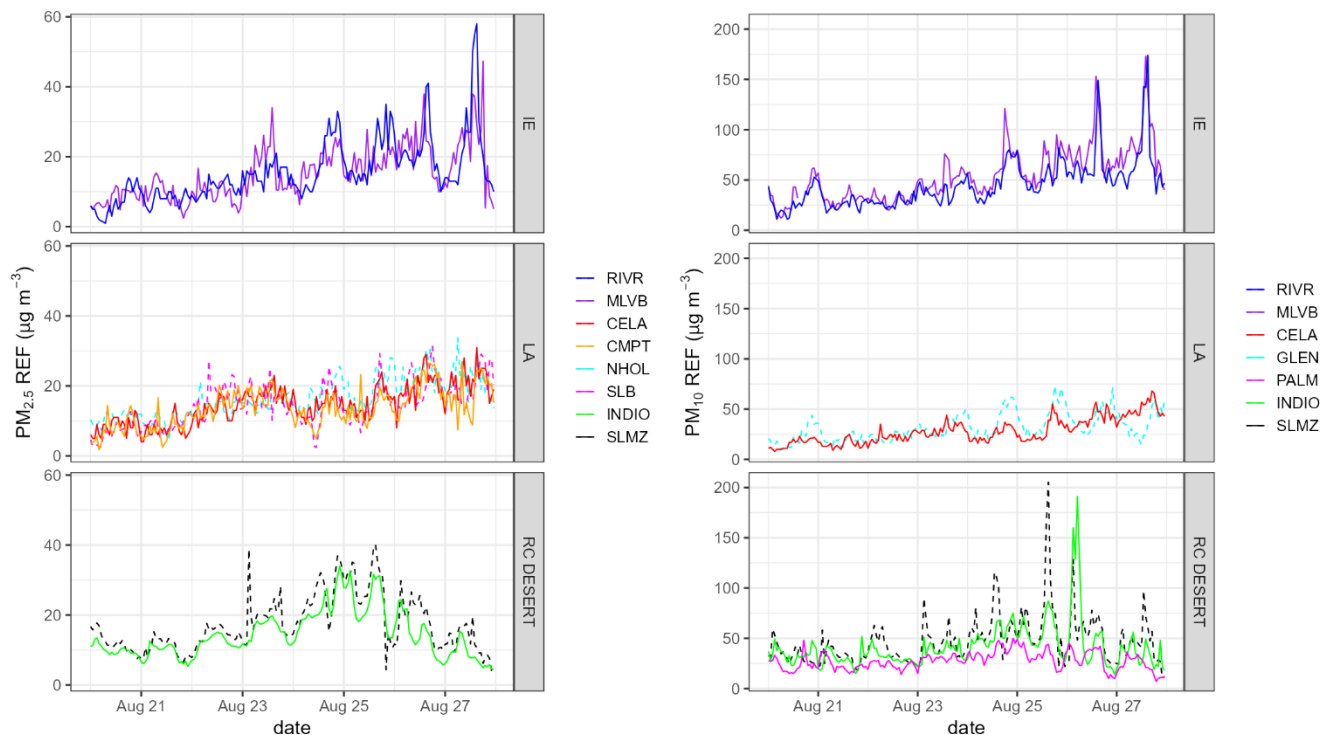
211

212 **3 Results and Discussion**

213 **3.1 General characteristics of the data**

214 $PM_{2.5}$ levels seem to be comparable across the sites and regions in LA and the IE, but lower levels were observed in the RC
215 Desert (Fig. S2). There are also distinct differences in the PM_{10} concentrations with higher levels observed in the IE (RIVR,
216 MLVB). $PM_{2.5}$ concentrations were highest in autumn and generally more variable over the autumn/winter period. The
217 timeseries shown in Fig. 2 show that while short-term local effects are visible (particularly for PM_{10} in the IE and RC Desert),
218 overall diurnal $PM_{2.5}$ and PM_{10} variations across sites within the same region were similar. This suggests that MOMA could
219 be an effective calibration framework for PM since the underlying requirement, that the diurnal patterns of pollutants at the
220 proxy site and at the site to be calibrated are similar, seems to be met, particularly for $PM_{2.5}$. For PM_{10} , a more careful selection
221 of a suitable calibration window may be required, given the short-term local differences.

222



223

224 **Figure 2: PM_{2.5} and PM₁₀ reference timeseries for a 7-day period grouped by regions (i.e., IE, LA, RC Desert). Co-location test sites**
 225 **are the solid lines. Sites with dashed lines are proxy sites only.**

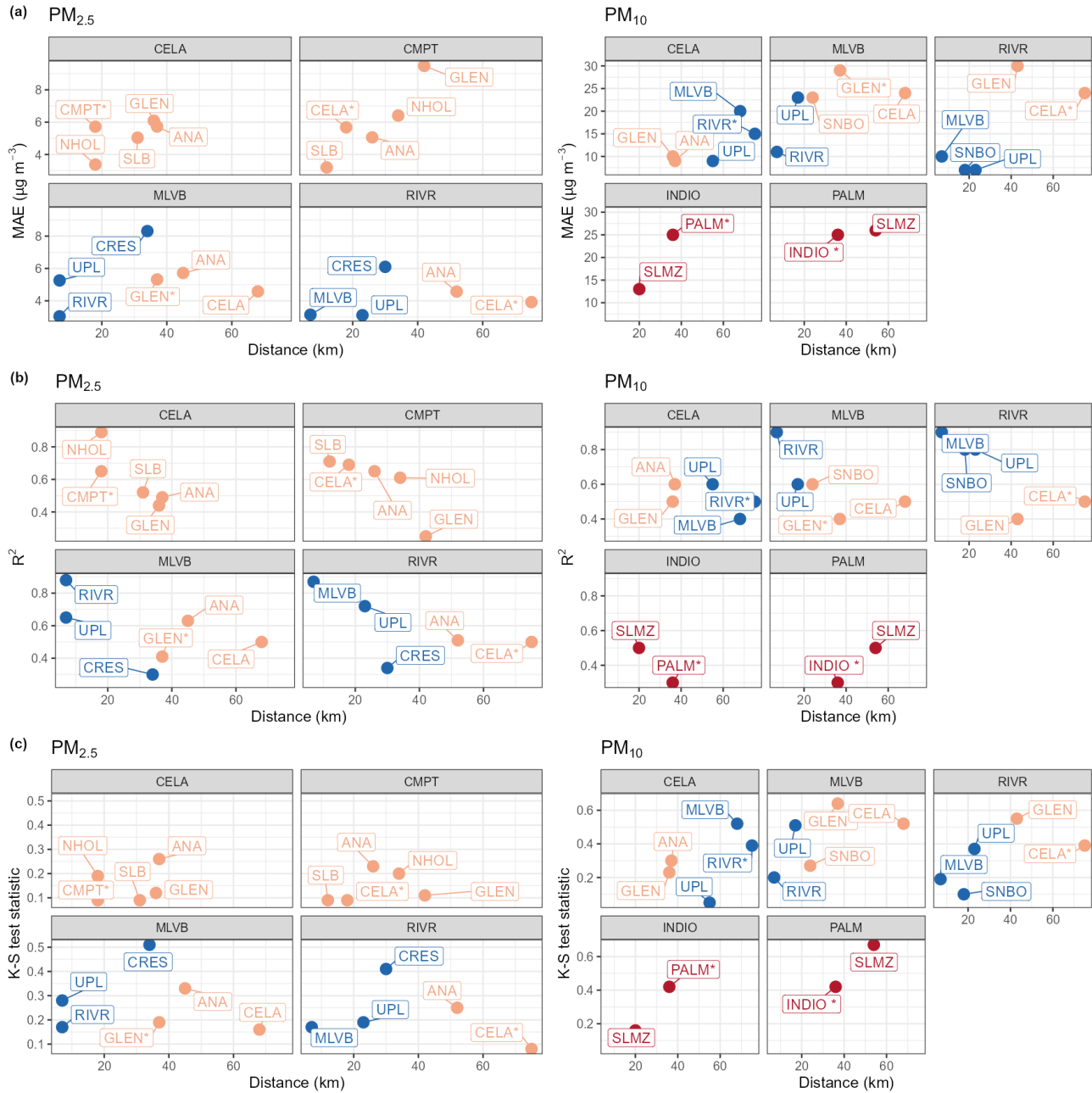
226

227 3.2 Proxy selection criteria

228 **Figure 3 shows the MAE, R^2 and K-S test statistic for proxies located at various distances away from the four (PM_{2.5}) and five**
 229 **(PM₁₀) co-located AMS test locations.** The figure demonstrates whether data obtained from the nearest site or the site with the
 230 most similar land use closely resemble the data at the respective test location. The figure illustrates that in most cases the
 231 nearest proxy site rather than the site with the most similar land proves to be the most appropriate proxy resulting in the lowest
 232 MAE and the highest R^2 throughout the entire year. Using the K-S test statistic as a measure of similarity across probability
 233 distributions reveals a slightly different pattern suggesting that PM_{2.5} CMPT or SLB may be more suitable proxies for CELA
 234 and that PM_{2.5} CELA could be a suitable proxy for MLVB or RIVR when upwind from MLVB or RIVR.

235 However, there are exceptions to this observation suggesting that other factors, such as PM sources associated with the
 236 surrounding land use, terrain, or prevailing wind direction, likely also contribute to the suitability of a proxy. For example, a
 237 proxy further away (CELA) seems to perform similarly to a nearby proxy (UPL) for PM_{2.5} at Mira Loma (MLVB). Mira
 238 Loma is downwind from CELA for most of the year, possibly explaining the low MAE against MLVB. The CRES site also
 239 seems to be a poorer PM_{2.5} proxy for MLVB and RIVR, which may be due to its location at higher altitudes as well as being
 240 separated from MLVB and RIVR by the San Bernardino mountains (1200+ meters high). Nevertheless, the nearest proxy

241 generally resulted in the most similar distribution with the lowest K-S test statistic, as well the lowest MAE and highest R^2 .
 242 Thus, we suggest selecting PM proxies based on distance for the following analysis as well as future deployments as long as
 243 the nearest proxy is within the same airshed (e.g. not separated by mountains).
 244



245
 246 **Figure 3: a) MAE, b) R^2 and c) K-S test statistic coloured by Region (LA: orange, IE: blue, RC Desert: red) for different proxies**
 247 **against distance to the co-located test location for PM_{2.5}: CELA, CMPT, MLVB, RIVR, and PM₁₀: CELA, MLVB, RIVR, INDIO,**

248 **PALM.** The site with the most similar land use to the test site is labelled with a ‘*’. The proxy site is labelled in each panel. The full
 249 site names are shown in Table 2. An ideal proxy would have a low MAE and K-S test statistic, as well as a high R^2 value. Proxies on
 250 the left hand side are closest to the co-located test location and therefore representative of the nearest proxies.

251

252 3.3 MOMA Calibration performance

253 The performance of MOMA was evaluated using sensors that were co-located at an AMS. Each sensor was mapped to its
 254 nearest proxy (Table 3), calibrated using the MOMA technique and compared to its co-located South Coast AQMD AMS
 255 using the metrics MAE, RMSE and R^2 .

256

257 **Table 3. List of AQYs co-located at South Coast AQMD AMS sites with their proxy reference sites.**

AMS ID	AQY Label	Region	PM _{2.5} Proxy	PM ₁₀ Proxy	Distance to PM _{2.5} Proxy (km)	Distance to PM ₁₀ Proxy (km)
RIVR	RIVR coloc	IE	MLVB	MLVB	7	7
MLVB	MLVB coloc	IE	RIVR	RIVR	7	7
CELA	CELA coloc	LA	NHOL	GLEN	12	36
CMPT	CMPT coloc	LA	SLB	*	18	
PALM	PALM coloc	RC Desert	*	INDIO		36
INDIO	INDIO coloc	RC Desert	SLMZ	SLMZ	21	21

258 * There is no PM₁₀ data available from CMPT and no PM_{2.5} measurement available from PALM

259
 260
 261
 262

Table 4. 24-hour averaged PM_{2.5} and PM₁₀ summary statistics for the AQYs against the co-located reference before the calibration (U), after the monthly calibration (M) and the drift calibration (D) over the 12-month period from Jan 2021 to Dec 2021.

AMS	Region	Mean Ref (SD) ($\mu\text{g m}^{-3}$)	Regression Slope			Regression Offset			R^2			MAE ($\mu\text{g m}^{-3}$)			RMSE ($\mu\text{g m}^{-3}$)			
			U	M	D	U	M	D	U	M	D	U	M	D	U	M	D	
PM_{2.5}	MLVB	IE	17 (8)	1.0	1.1	0.8	-4	-4	-1	0.7	0.5	0.7	6	7	6	7	9	6
	RIVR	IE	12 (8)	1.2	1.3	1.2	-4	2	2	0.9	0.6	0.8	4	5	6	5	10	8
	CELA	LA	15 (7)	0.3	0.8	0.8	0	4	3	0.4	0.4	0.7	9	11	4	11	6	4
	CMPT	LA	14 (7)	0.9	1.8	1.1	-4	-8	-1	0.7	0.6	0.8	6	7	6	7	11	4
	INDIO	RC Desert	9 (4)	0.4	0.9	1.2	0	3	0	0.6	0.5	0.5	6	6	3	6	4	5
				U	M	D	U	M	D	U	M	D	U	M	D	U	M	D
PM₁₀	MLVB	IE	51 (25)	0.3	0.4	0.5	7	23	17	0.2	0.2	0.4	28	20	14	34	30	22
	RIVR	IE	40 (18)	0.6	1.4	1.1	-4	2	7	0.4	0.3	0.6	21	22	12	25	44	18
	CELA	LA	31 (12)	0.4	0.7	0.7	1	6	6	0.4	0.4	0.4	19	9	8	21	12	12
	INDIO	RC Desert	48 (38)	0.1	0.5	0.6	7	28	23	0.5	0.4	0.4	36	18	18	49	31	31
	PALM	RC Desert	23 (11)	0.3	1.4	1.3	1	7	5	0.6	0.2	0.4	16	21	14	18	39	21

263 3.3.1 PM_{2.5}

264 Table 4 shows the 24-hour averaged PM_{2.5} and PM₁₀ summary statistics for the AQYs against the co-located reference before
265 the calibration (gain = 1, offset = 0 + RH correction) (U), after the monthly calibration (M) and the drift calibration (D) over
266 the 12-month period from Jan 2021 to Dec 2021. The monthly MAE are shown in Figure 4.

267 The sensors in the LA and the RC Desert Region were under-reading PM_{2.5} concentrations prior to calibration, this was
268 particularly evident for the AQY co-located at the INDIO AMS (slope: 0.4). These sensors show a clear improvement with
269 both the monthly and drift calibration applied as indicated by a slope closer to 1 and an up to 60% reduction in the MAE and
270 RMSE, although the improvement varies across the sensors (Table 4). The monthly and drift calibrations did not improve the
271 R^2 or slope for the sensors in the IE at MLVB and RIVR. Unlike the AQYs in the LA Region or the RC Desert the uncalibrated
272 data showed a strong correlation with the co-located reference R^2 (0.7/0.9) and the slope (1.0/1.2) and MAE (4 - 6 $\mu\text{g m}^{-3}$) were
273 already within the range of calibrated slopes and MAE. This suggests that the standard factory sensor calibration transferred
274 well to the field at MLVB and RIVR. Calibrating the sensor data against the proxy however, seemed to have introduced errors.
275 There are several reasons for this. Firstly, Fig. 4 shows that the MAE between the co-located reference data and the proxy data
276 is larger at RIVR than the MAE for the uncalibrated data against the co-located reference data indicating that the MLVB proxy
277 was not always suitable for MOMA calibration of the RIVR sensor. This is also supported by the differing probability
278 distributions from the two sites (Fig. S3) which suggests the sites were exposed to different PM levels. On the other hand, the
279 probability distributions for CELA and NHOL PM_{2.5} data and that for CMPT and SLB were very similar (Fig. S3) and hence
280 the MOMA calibration process produced improved accuracy.

281 Secondly, monthly variability in particle source and composition will impact the reliability of the MOMA calibration
282 particularly for those performed at monthly intervals. For example, the very high monthly MOMA MAE for February at CELA,
283 MLVB and RIVR suggests the January particle composition was not representative of that observed in February at these sites.
284 Particle composition is known to vary with different wind directions (desert vs. marine/urban particles) and impact the sensor
285 reading as observed in previous studies (Castell et al., 2017; Gao et al., 2015; Giordano et al., 2021; Kelly et al., 2017). The
286 effect of this phenomenon is particularly visible between November and February when wind was more variable. This is
287 supported by Fig. 4, which shows that for both the LA and IE regions the MAE tended to be higher in November/December
288 and January for uncalibrated as well as calibrated data. The difference between the proxy and the co-located reference data
289 also tended to be larger during these months.

290 A similar month-to-month variability in the MAE can be observed when comparing the reference monitor (BAM 1020, Met
291 One Instruments, Inc., Grants Pass, Oregon, US) at RIVR against the reference grade optical instruments T640 (Teledyne API,
292 San Diego, US) and the GRIMM optical particle counter (EDM 180, GRIMM Aerosol Technik GmbH & Co., Airing,
293 Germany), also located at the RIVR site. The T640 and GRIMM are both optical particle counter instruments that determine
294 the aerosol particle size distribution from which they estimate the PM concentration. The BAM-1020 samples aerosols through
295 a PM₁₀ inlet and uses a Very Sharp Cut Cyclone (VSCC) to classify it into PM_{2.5} before collecting it on a filter tape and
296 determining the PM_{2.5} concentration by the aerosol's attenuation of a C₁₄ beta radiation source (Hagler et al., 2022). Due to the

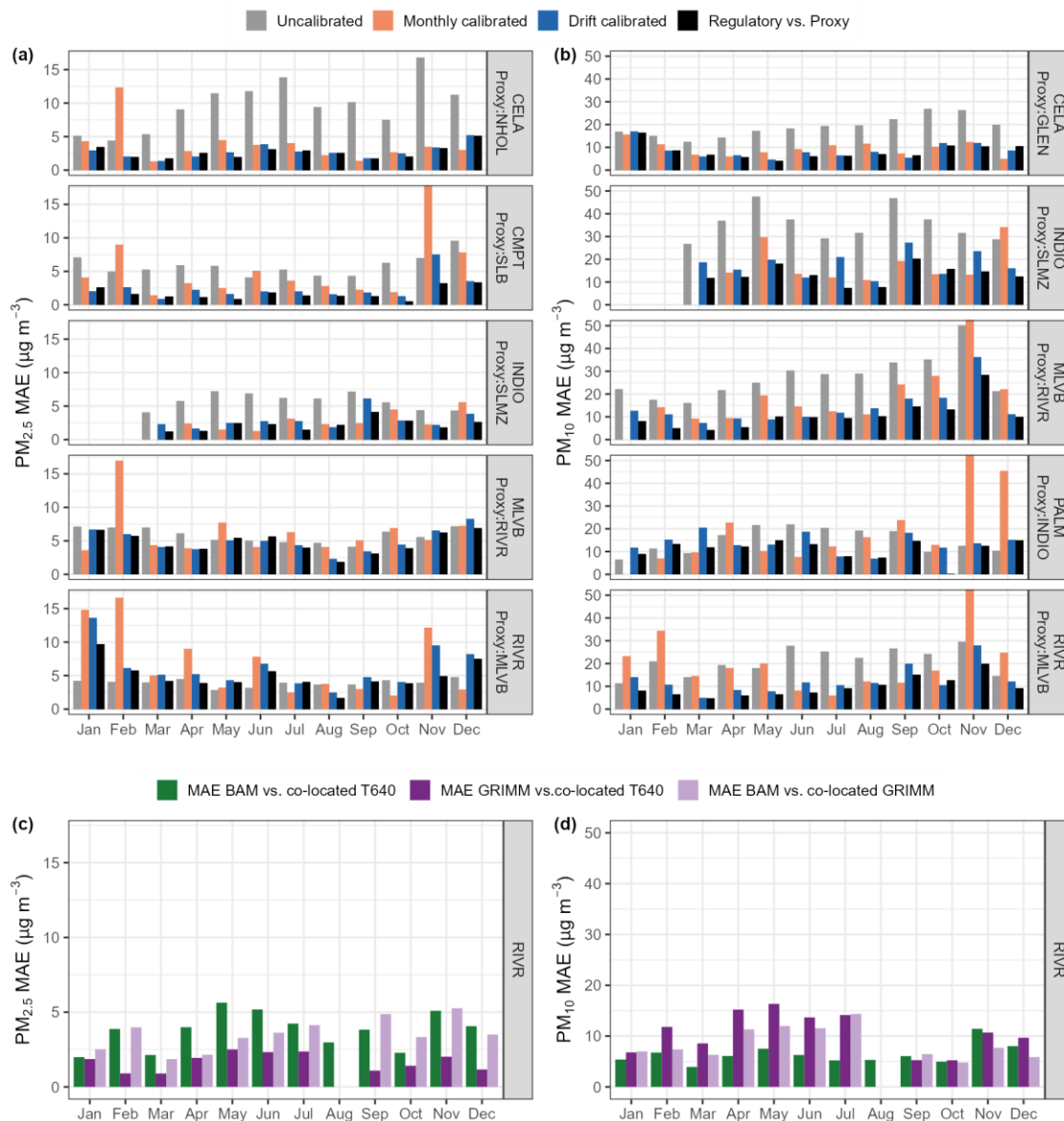
297 differences in the measurement principles, the instruments can give different results depending on the properties of the
298 measured particles.

299 The T640 and GRIMM match each other consistently across the year (similar technologies) but the BAM/T640 and
300 BAM/GRIMM MAE were higher in general and highest during the November/December months. This further shows how
301 differences between measurement technologies will be exacerbated when particle composition is variable. This is discussed in
302 more detail in sect. 3.5.

303 Thirdly, measurement noise in the hourly reference data from the beta attenuation monitors deployed at the sites may be too
304 high to reliably calibrate low-cost sensors when concentrations are low ($< 40 \mu\text{g m}^{-3}$) as often was the case in the RC Desert
305 (Hagler et al., 2022; Johnson et al., 2018; Zheng et al., 2018). The calibration improved the data most during the summer
306 months with the MAE equal or below $5 \mu\text{g m}^{-3}$.

307

308



309

310 **Figure 4: Bar charts showing the uncalibrated (gain = 1, offset = 0 + RH correction, monthly calibrated and drift calibrated MAE**
 311 **between the AQY 24-hour averaged $\text{PM}_{2.5}$ (a) / PM_{10} (b) and the co-located reference. For comparison it also shows the MAE between**
 312 **the proxy reference and the co-located reference in black. (c) and (d) show the MAE between the 24-hour averaged BAM and co-**
 313 **located T640, the GRIMM and the co-located T640 and the BAM and the co-located GRIMM.**

314 3.3.2 PM_{10}

315 **As expected, the PM_{10} data from the sensors generally showed a poorer agreement with the co-located reference with a high**
 316 **MAE ($16 - 36 \mu\text{g m}^{-3}$) and RMSE ($18 - 49 \mu\text{g m}^{-3}$) and low R^2 ($0.2 - 0.6$) (Table 4) for uncalibrated data. The uncalibrated**

317 data were also underestimating PM_{10} concentrations, particularly in the RC Desert (INDIO, PALM) as shown by the low slope
318 (0.1 – 0.3). This is in agreement with previous work which showed that the SDS011 underestimates PM_{10} , particularly for
319 particles greater than $5\ \mu m$ which dominate in the RC Desert (Budde et al., 2018; Kuula et al., 2020; Ostro et al., 2000).

320 The monthly and drift triggered MOMA calibrations had a clear positive impact on PM_{10} and improved the accuracy as
321 indicated by a nearly 60% decrease in the MAE and a 40% decrease in the RMSE in the LA Region (CELA) (Table 4).
322 However, the scatter remained and resulted in no improvement in the R^2 . The drift detection framework also improved the
323 accuracy of the data at the two AQYs located in the IE. The monthly calibrations, on the other hand, decreased the accuracy
324 at RIVR where the MAE and RMSE were higher after the calibration compared to uncalibrated data (Table 4).

325 The Proxy/REF MAE (Fig. 4) was highest in the RC Desert suggesting that the SLMZ is not a suitable proxy for PM_{10} at
326 INDIO. To some extent this is expected since the PM coarse fraction ($PM_{10} - PM_{2.5}$) is more dominated by local sources than
327 $PM_{2.5}$ (Pinto et al., 2004).

328 However, similar to $PM_{2.5}$, there was month-to-month variability in the calibration performance, with better improvements
329 during summer and poor performance in November, particularly in the IE and RC Desert (Fig. 4). Potential factors that
330 contribute to the high MAE in November are further discussed in sect. 3.5.

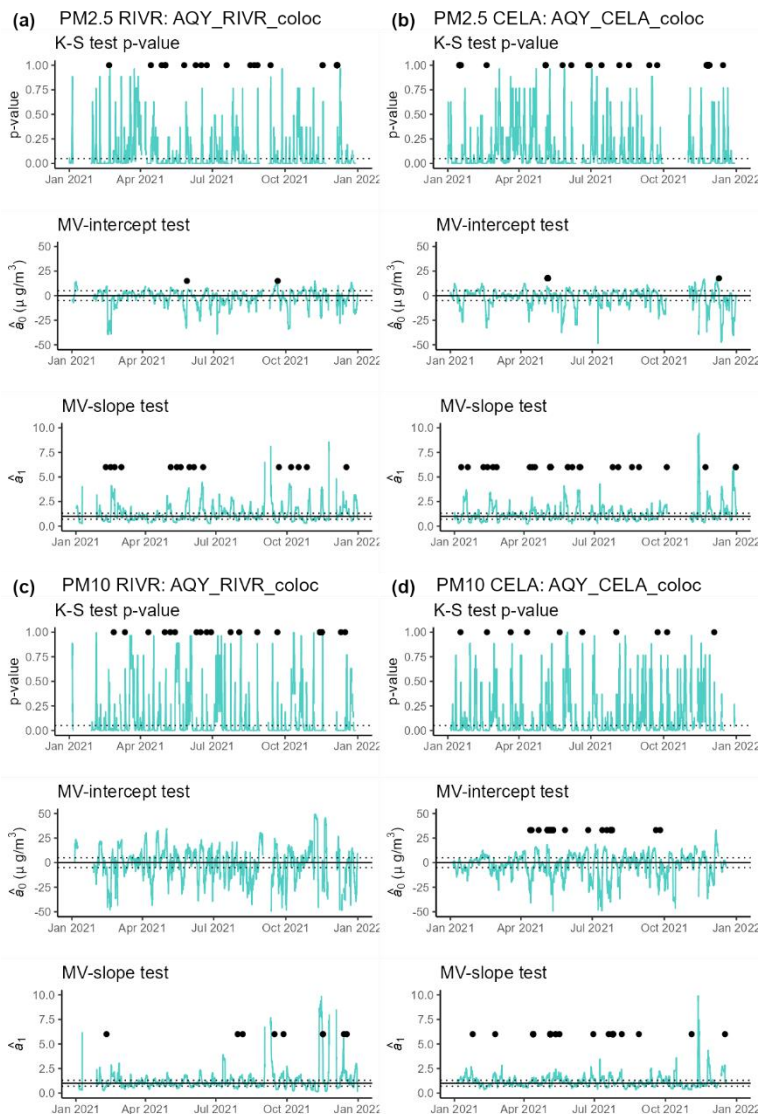
331 A comparison of the PM_{10} data from the reference instruments at RIVR (BAM, GRIMM, T640) shows that the MAE across
332 different instrument types can be as high as $\sim 15\ \mu g\ m^{-3}$ and the GRIMM and T640 PM_{10} MAE is the highest – the opposite of
333 the $PM_{2.5}$ result. This observation illustrates the importance of the assumptions used to relate signal to aerodynamic radius and
334 mass, which are different for different instrument types.

335

336 3.4 Drift detection triggers

337 The results from the drift detection framework tests are shown in Fig. 5 (K-S test p-value, MV-slope test, \hat{a}_1 , and the MV-
338 intercept test, \hat{a}_0) for $PM_{2.5}$ and PM_{10} measured by a PM sensor deployed in the LA region and one in the IE region. The black
339 points indicate when the framework triggered a drift alarm and calibration. It is evident that most alarms were raised due to
340 significant differences in the probability distributions (K-S test p-value < 0.05), followed by a change in the slope between the
341 proxy and sensor (MV-slope test). Alarms triggered by the K-S test are spread across the whole year but generally more
342 common during the summer months, possibly concentrations are lower then, so instrument noise becomes important and is
343 determining the signal distribution across the observed range. In the IE (RIVR) alarms related to changes in the MV-slope
344 were clustered around February, May, and September/October suggesting more frequent changes in environmental conditions
345 (e.g., RH) or particle composition and size during these months (discussed in sect. 3.5). The AQY sensor installed at the CELA
346 AMS sent off alarms that were more spread across the whole year suggesting that sensor drift at this site was not related to
347 seasons. The figure also shows that there are frequent calibrations within a month at both sites likely due to within month
348 changes in meteorological and environmental conditions (discussed in sect. 3.5). This partly explains the better performance
349 of the drift calibrated data compared to the monthly calibrated data.

350

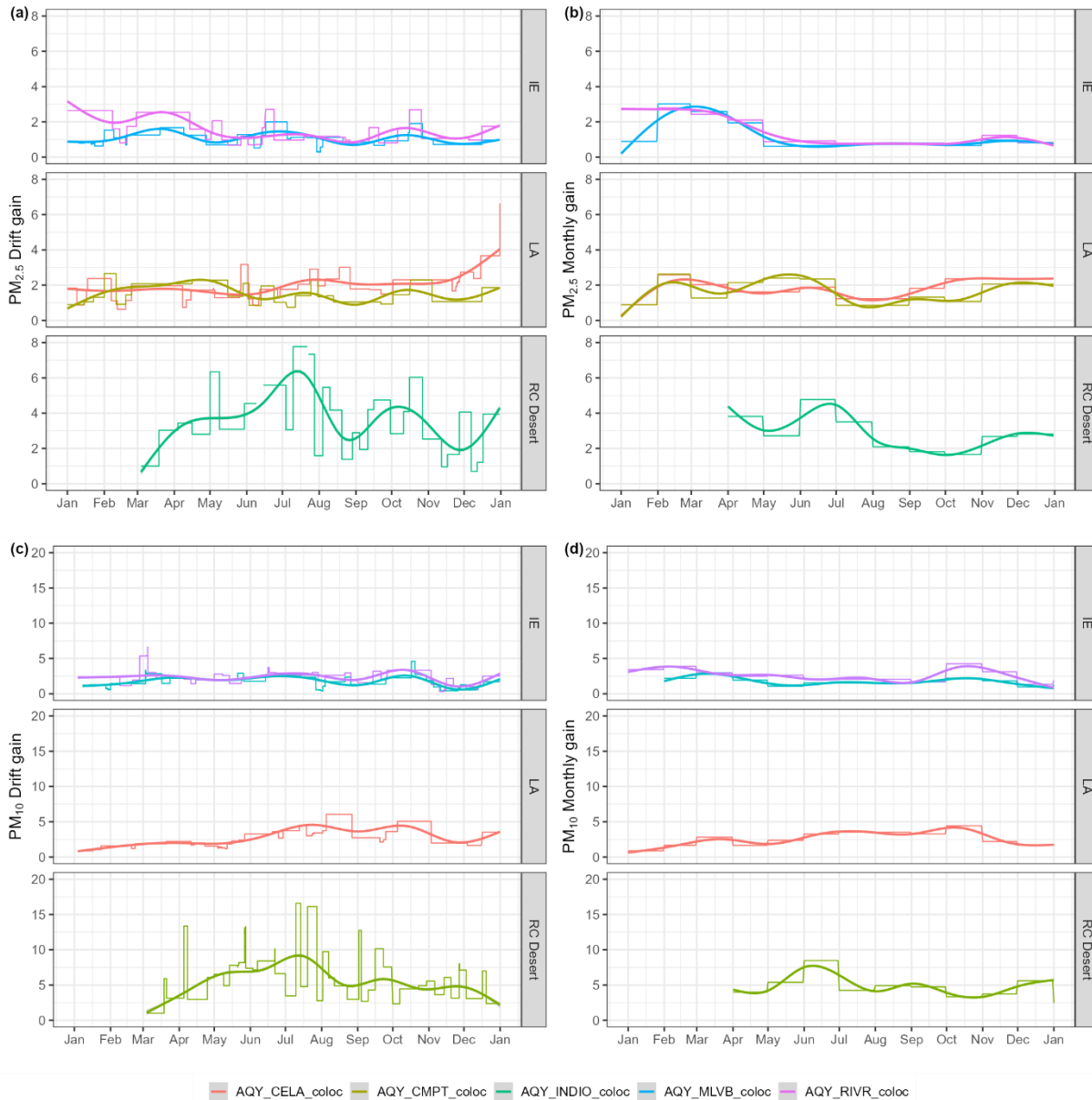


351

352 **Figure 5: Test statistics from drift detection framework for a site in the IE (a) / (c) and one in the City of LA region (b) / (d) for PM_{2.5}**
 353 **and PM₁₀, respectively. The black points show when the drift detection framework resulted in an alarm and triggered a calibration.**
 354 **The dotted lines represent the thresholds used to trigger a drift alarm: K-S test p-value < 0.05; $-5 \mu\text{g m}^{-3} > \hat{a}_0 > 5 \mu\text{g m}^{-3}$, $0.75 > \hat{a}_1 >$**
 355 **1.25. A drift alarm (black dot) was triggered when thresholds were exceeded for consecutive 5 days.**

356 Figure 6 shows the temporal variability of monthly and drift calculated gains for sensors in the IE, LA and RC Desert Region.
 357 The temporal variation of the PM_{2.5} and PM₁₀ gains calculated by the monthly calibrations (Fig. 6. (b)/(d)) show a distinct
 358 seasonal pattern with higher gains (~2-3) during autumn and winter and lower gains (~1) during the summer months,
 359 particularly in the IE region. An opposite pattern is visible in the RC Desert where gains were not only reaching a maximum
 360 over the summer months but were also around six times higher than those in the IE or LA region. The gains from the drift

361 detection framework were more variable as visible from the more frequent step changes but also showed some seasonal
 362 dependence. These results suggest that unlike calibrating for sensor drift (which would be shown as a continuous increase in
 363 the slope over time as observed when calibrating O₃ Sensors (Miskell et al., 2019)) PM sensors are calibrated for different
 364 conditions, which can vary frequently as shown by the step changes of the drift gains.



365

366 **Figure 6: Temporal variation of the gains as calculated from the drift detection framework (a) and the monthly calibrations (b) for**
 367 **PM_{2.5} and PM₁₀ (c) and (d), respectively. Step changes refer to a change in the calibration gain and a smooth curve was fitted through**
 368 **the data points to visualise the overall temporal trend of the gains.**

369

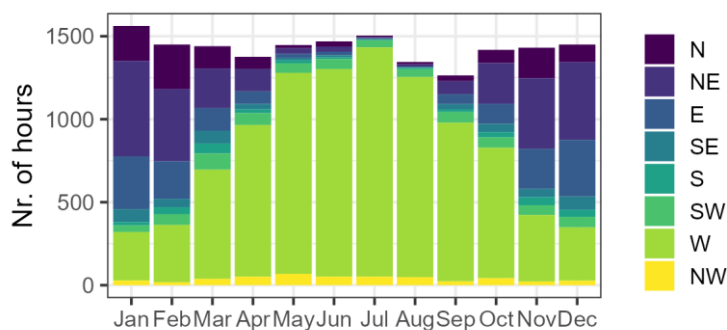
370 3.5 Particle composition variability

371 As observed in the previous sections, calibrating PM sensors can be challenging in complex areas where particle composition,
372 size and physical properties (i.e., shape and refractive index) vary spatially and temporally (Kuula et al., 2020). In this section,
373 we discuss some of the origins for the variations in particle composition with a specific focus on the Riverside area (RIVR
374 AMS).

375 The wind data from Riverside Municipal airport wind data shown in Fig. 7, clearly indicates the seasonal variation in the wind
376 direction with N/NE winds dominating during the late autumn/winter months and W winds dominating during the rest of the
377 year. It is also visible that wind is more variable in late fall/winter possibly explaining the more frequent alarms observed for
378 these months at Riverside (Fig. 5). The N/NE winds correspond to the SAW which are associated with very dry downslope air
379 flow from the northeast and common between October and April, with a peak in December and January (Aguilera et al., 2020).
380 Typically, PM concentrations during SAW conditions are dominated by coarse particles of crustal components (Guazzotti et
381 al., 2001; Qin et al., 2012).

382

383



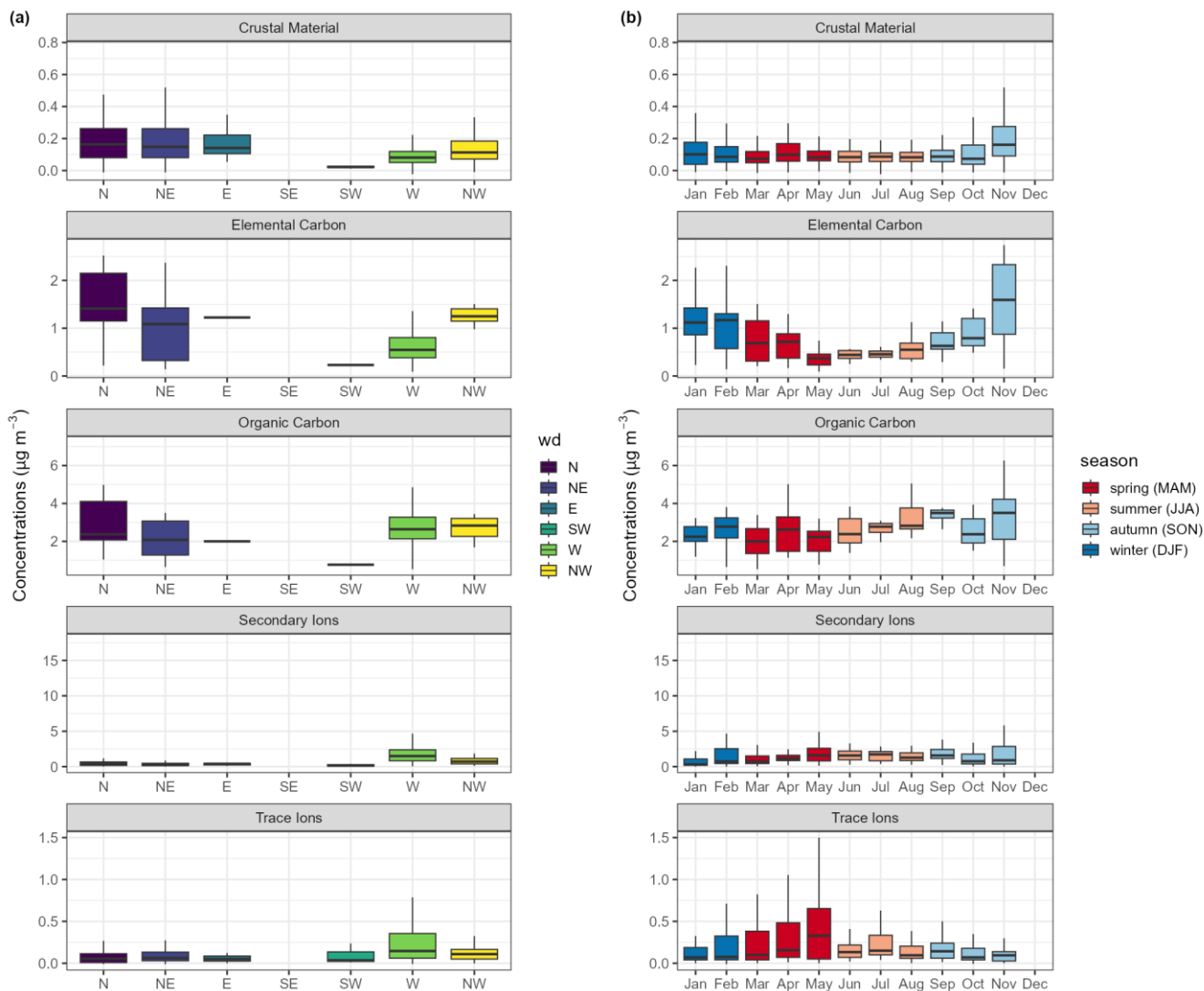
384

385 **Figure 7: Nr. of hours dominated by different wind direction measured at Riverside Municipal Airport during each month.**

386

387 This is in agreement with observations from Fig. 8 which shows higher concentrations of Crustal Material and Elemental
388 Carbon during N/NE and NW, reaching a maximum in November. Organic Carbon concentrations, likely driven by traffic
389 emissions are similar across the dominant wind directions with maximum concentrations observed in November. Higher
390 autumn and winter OC concentrations have previously also been observed by Daher et al. (2012) and were explained by
391 stronger atmospheric stability which restricted atmospheric mixing. Higher concentrations of OC observed over the summer
392 months when EC concentrations were low are likely due to increased PM advection and secondary organic aerosol formation
393 as commonly observed for the inland locations downwind from urban sites (Daher et al., 2013). Trace ions (Chloride, Sodium

394 and Potassium ion) and secondary ions (nitrate, sulfate, ammonium), on the other hand, are highest downwind from the City
 395 of LA reaching a maximum in spring/summer due to increased photochemical activity and a larger contribution of sulfate
 396 sources and its precursor (fuel/ship emissions) upwind of the City of LA (Daher et al., 2013).



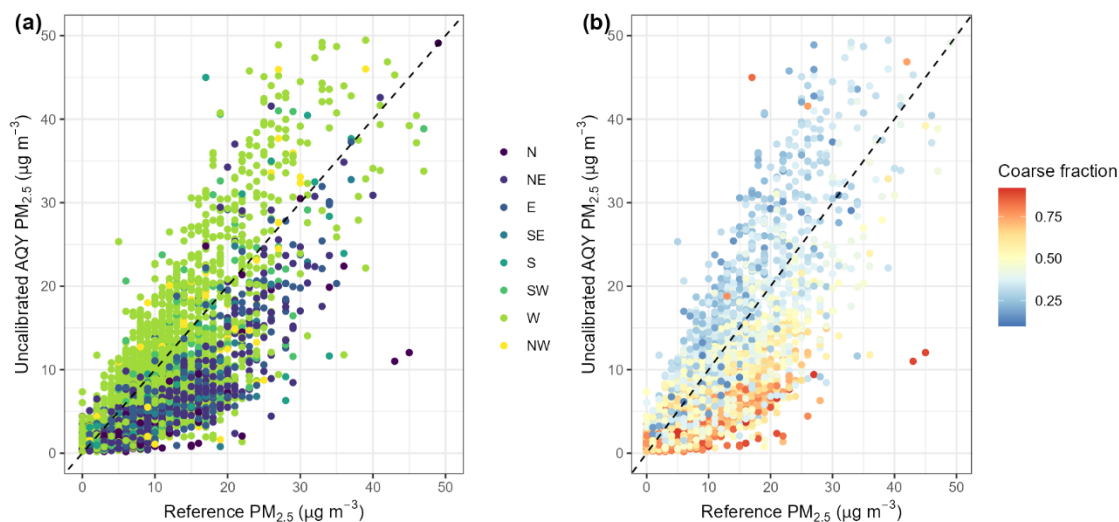
397

398 **Figure 8: Boxplots showing speciation concentrations collected at AMS – Rubidoux (RIVR) grouped into 5 categories (Panels)**
 399 **plotted against wind direction (wd) (a) and for each month of the year coloured by different seasons (b). Note – there was no data**
 400 **for SE winds which were not common during the study period. The lower and upper hinges represent the 25th and 75th percentiles**
 401 **with the median marked inside the box. The lower and upper whiskers extend 1.5*inter-quartile range from the hinge.**

402

403 Figure 9 illustrates the relationship between the BAM and co-located sensor data coloured by wind direction and course
 404 fraction ($1 - \text{PM}_{2.5}/\text{PM}_{10}$). The figure reveals a clear slope dependence on the wind direction (<1 when wind was from a
 405 northeast origin and ≥ 1 when wind from a western origin dominated), suggesting that it underestimates $\text{PM}_{2.5}$ levels during
 406 north-eastern wind (SAW conditions). These conditions correspond to a higher proportion of coarse fraction, likely associated
 407 with Crustal Material, further highlighting that the AQY is underestimating larger particles (Fig. 9b). In fact, Budde et al.
 408 (2018) found that the SDS011 used in this study strongly underestimates particles $> 2 \mu\text{m}$ in the $\text{PM}_{2.5}$ measurement.

409



410

411 **Figure 9: Hourly uncalibrated low-cost sensor data against hourly co-located reference data at AMS - Rubidoux (RIVR) during**
 412 **2021, a) coloured by wind direction, b) coloured by the AQY PM coarse fraction: $1 - \text{PM}_{2.5}/\text{PM}_{10}$.**

413 4 Conclusions and future work

414 This work is part of a large study set out to determine if a remote calibration framework (MOMA), previously developed for
 415 the correction of drift in O_3 and NO_2 sensors (Miskell et al., 2018, 2019; Weissert et al., 2020) can be applied for $\text{PM}_{2.5}$ and
 416 PM_{10} data from PM sensors. We identified suitable reference proxies based on distance and presented two approaches to
 417 remotely calibrate data from sensor networks, 1) at monthly intervals and 2) using a drift detection framework that triggers a
 418 calibration when drift is detected. Our results show that averaged across all seasons and sites MOMA reduces the $\text{PM}_{2.5}$ RMSE
 419 from 8 to $5 \mu\text{g m}^{-3}$ with average $\text{PM}_{2.5}$ concentrations of $13 \mu\text{g m}^{-3}$. This is comparable to the improvement achieved from a
 420 global correction applied to PurpleAir sensors where the 24-hour averaged $\text{PM}_{2.5}$ RMSE was reduced from 8 to $3 \mu\text{g m}^{-3}$
 421 (average $\text{PM}_{2.5}$ reference concentration: $9 \mu\text{g m}^{-3}$) (Barkjohn et al., 2021). While both the monthly and drift calibration
 422 improved the accuracy of the data on average, the drift correction framework performed better. Overall, the improvement due

423 to the MOMA calibration was more obvious for PM₁₀ with an overall reduction in the RMSE from 30 to 21 $\mu\text{g m}^{-3}$ at average
424 PM₁₀ reference concentrations of 39 $\mu\text{g m}^{-3}$.

425 We note that calibrating PM sensors is more challenging than calibrating gas sensors (e.g. O₃, Miskell et al. 2019, NO₂,
426 Weissert et al. (2020)) due to the spatial and temporal variations of particle composition and the resulting differences in
427 response between the reference BAM instruments and the PM sensors. This was visible in the IE where particle composition
428 varied between desert dust (N/NE) and marine/urban aerosol (W) during the winter months, meaning that the monthly
429 calibration applied forward may not be correct and data should be interpreted with caution. This also highlights that a more
430 flexible proxy selection approach depending on dominant wind direction and particle source may be more suitable than using
431 the same proxy site across all seasons.

432 Since the optical PM sensor accuracy depends on the atmospheric aerosol composition it is expected that MOMA with the
433 drift detection framework has an advantage over other methods such as calibration by co-location or using a mobile reference
434 in that it is continuous whereas the other methods are performed at discrete time periods and do not account for aerosol
435 composition changes between calibrations. Future work will focus on optimising MOMA and apply it to other PM sensors
436 (e.g. PurpleAir sensors) (Collier-Oxandale, to be submitted).

437

438 **Appendix**

439 Supplementary Information

440

441 **Data and code availability**

442 10-min, 1-hr, and 24-hr averaged data from the SCAQMD sensor network can be exported from <https://aqportal.aqmd.gov/>.

443 The code is not publicly accessible due to intellectual property.

444

445 **Author contributions**

446 G.S.H., D.E.W., V.P. formulation of overarching research goals and aims.; D.E.W., L.F.W. and G.S.H. developed the
447 methodology; B.F., A.C.-O. and R.L. managed and maintained the sensor network, L.F.W. developed the software and
448 performed the data analysis, L.F.W. prepared the manuscripts with contributions from all co-authors. V.P., A.P. and G.S.H.
449 supervised the project.

450

451 **Competing interests**

452 The authors declare the following financial interests/personal relationships which may be considered as potential competing
453 interests: L.F.W. and G.S.H. are employees of Aeroqual Ltd, manufacturer of the sensor nodes used in these studies. G.S.H. and
454 D.E.W. are founders and shareholders in Aeroqual Ltd.

455 **References**

- 456 Aguilera, R., Gershunov, A., Ilango, S. D., Guzman-Morales, J., and Benmarhnia, T.: Santa Ana Winds of Southern California
457 Impact PM_{2.5} With and Without Smoke From Wildfires, *GeoHealth*, 4, <https://doi.org/10.1029/2019GH000225>, 2020.
- 458 Anderson, J. O., Thundiyil, J. G., and Stolbach, A.: Clearing the Air: A Review of the Effects of Particulate Matter Air Pollution
459 on Human Health, *J. Med. Toxicol.*, 8, 166–175, <https://doi.org/10.1007/s13181-011-0203-1>, 2012.
- 460 Aphalo, P. J., Slowikowski, K., and Mouksassi, S.: ggpmisc: Miscellaneous Extensions to “ggplot2,” 2022.
- 461 Atkinson, R. W., Fuller, G. W., Anderson, H. R., Harrison, R. M., and Armstrong, B.: Urban Ambient Particle Metrics and
462 Health: A Time-series Analysis, *Epidemiology*, 21, 501–511, <https://doi.org/10.1097/EDE.0b013e3181debc88>, 2010.
- 463 Badura, M., Batog, P., Drzeniecka-Osiadacz, A., and Modzel, P.: Evaluation of Low-Cost Sensors for Ambient PM_{2.5}
464 Monitoring, *J. Sens.*, 2018, 1–16, <https://doi.org/10.1155/2018/5096540>, 2018.
- 465 Barkjohn, K. K., Gantt, B., and Clements, A. L.: Development and application of a United States-wide correction for
466 PM_{2.5} data collected with the PurpleAir sensor, *Atmospheric Meas. Tech.*, 14, 4617–4637,
467 <https://doi.org/10.5194/amt-14-4617-2021>, 2021.
- 468 Budde, M., Schwarz, A. D., Mueller, T., Laquai, B., Streibl, N., Schindler, G., Koepke, M., Riedel, T., Dittler, A., and Beigl,
469 M.: Potential and Limitations of the Low-Cost SDS011 Particle Sensor for Monitoring Urban Air Quality | ProScience, in:
470 ProScience, 3rd International Conference on Atmospheric Dust - DUST2018, 6–12, 2018.
- 471 California Air Resources Board: Inhalable Particulate Matter and Health (PM_{2.5} and PM₁₀), 2023,
472 <https://ww2.arb.ca.gov/resources/inhalable-particulate-matter-and-health>, Accessed: 31.07.2023.
- 473 Carslaw, D.: worldmet: Import Surface Meteorological Data from NOAA Integrated Surface Database (ISD), 2022.
- 474 Carslaw, D. and Ropkins, K.: openair: Tools for the Analysis of Air Pollution Data, 2022.
- 475 Castell, N., Dauge, F. R., Schneider, P., Vogt, M., Lerner, U., Fishbain, B., Broday, D., and Bartonova, A.: Can commercial
476 low-cost sensor platforms contribute to air quality monitoring and exposure estimates?, *Environ. Int.*, 99, 293–302,
477 <https://doi.org/10.1016/j.envint.2016.12.007>, 2017.
- 478 Crilley, L. R., Shaw, M., Pound, R., Kramer, L. J., Price, R., Young, S., Lewis, A. C., and Pope, F. D.: Evaluation of a low-
479 cost optical particle counter (Alphasense OPC-N2) for ambient air monitoring, *Atmospheric Meas. Tech.*, 11, 709–720,
480 <https://doi.org/10.5194/amt-11-709-2018>, 2018.
- 481 Crilley, L. R., Singh, A., Kramer, L. J., Shaw, M. D., Alam, M. S., Apte, J. S., Bloss, W. J., Hildebrandt Ruiz, L., Fu, P., Fu,
482 W., Gani, S., Gatari, M., Ilyinskaya, E., Lewis, A. C., Ng’ang’a, D., Sun, Y., Whitty, R. C. W., Yue, S., Young, S., and Pope,
483 F. D.: Effect of aerosol composition on the performance of low-cost optical particle counter correction factors, *Atmospheric*
484 *Meas. Tech.*, 13, 1181–1193, <https://doi.org/10.5194/amt-13-1181-2020>, 2020.
- 485 Daher, N., Hasheminassab, S., Shafer, M. M., Schauer, J. J., and Sioutas, C.: Seasonal and spatial variability in chemical
486 composition and mass closure of ambient ultrafine particles in the megacity of Los Angeles, *Env. Sci Process. Impacts*, 15,
487 283–295, <https://doi.org/10.1039/C2EM30615H>, 2013.

488 De Vito, S., Esposito, E., Castell, N., Schneider, P., and Bartonova, A.: On the robustness of field calibration for smart air
489 quality monitors, *Sens. Actuators B Chem.*, 310, 127869, <https://doi.org/10.1016/j.snb.2020.127869>, 2020.

490 Eeftens, M., Beelen, R., de Hoogh, K., Bellander, T., Cesaroni, G., Cirach, M., Declercq, C., Dèdelè, A., Dons, E., de Nazelle,
491 A., Dimakopoulou, K., Eriksen, K., Falq, G., Fischer, P., Galassi, C., Gražulevičienė, R., Heinrich, J., Hoffmann, B., Jerrett,
492 M., Keidel, D., Korek, M., Lanki, T., Lindley, S., Madsen, C., Mölter, A., Nádor, G., Nieuwenhuijsen, M., Nonnemacher, M.,
493 Pedeli, X., Raaschou-Nielsen, O., Patelarou, E., Quass, U., Ranzi, A., Schindler, C., Stempfelet, M., Stephanou, E., Sugiri, D.,
494 Tsai, M.-Y., Yli-Tuomi, T., Varró, M. J., Vienneau, D., Klot, S. von, Wolf, K., Brunekreef, B., and Hoek, G.: Development
495 of Land Use Regression Models for PM_{2.5}, PM_{2.5} Absorbance, PM₁₀ and PM_{coarse} in 20 European Study Areas; Results of
496 the ESCAPE Project, *Environ. Sci. Technol.*, 46, 11195–11205, <https://doi.org/10.1021/es301948k>, 2012.

497 Feng, S., Gao, D., Liao, F., Zhou, F., and Wang, X.: The health effects of ambient PM_{2.5} and potential mechanisms,
498 *Ecotoxicol. Environ. Saf.*, 128, 67–74, <https://doi.org/10.1016/j.ecoenv.2016.01.030>, 2016.

499 Gao, M., Cao, J., and Seto, E.: A distributed network of low-cost continuous reading sensors to measure spatiotemporal
500 variations of PM_{2.5} in Xi'an, China, *Environ. Pollut.*, 199, 56–65, <https://doi.org/10.1016/j.envpol.2015.01.013>, 2015.

501 Giordano, M. R., Malings, C., Pandis, S. N., Presto, A. A., McNeill, V. F., Westervelt, D. M., Beekmann, M., and Subramanian,
502 R.: From low-cost sensors to high-quality data: A summary of challenges and best practices for effectively calibrating low-
503 cost particulate matter mass sensors, *J. Aerosol Sci.*, 158, 105833, <https://doi.org/10.1016/j.jaerosci.2021.105833>, 2021.

504 Guazzotti, S. A., Whiteaker, J. R., Suess, D., Coffee, K. R., and Prather, K. A.: Real-time measurements of the chemical
505 composition of size-resolved particles during a Santa Ana wind episode, California USA, *Atmos. Environ.*, 35, 3229–3240,
506 [https://doi.org/10.1016/S1352-2310\(01\)00140-6](https://doi.org/10.1016/S1352-2310(01)00140-6), 2001.

507 Hagler, G., Hanley, T., Hassett-Sipple, B., Vanderpool, R., Smith, M., Wilbur, J., Wilbur, T., Oliver, T., Shand, D., Vidacek,
508 V., Johnson, C., Allen, R., and D'Angelo, C.: Evaluation of two collocated federal equivalent method PM_{2.5} instruments over
509 a wide range of concentrations in Sarajevo, Bosnia and Herzegovina, *Atmospheric Pollut. Res.*, 13, 101374,
510 <https://doi.org/10.1016/j.apr.2022.101374>, 2022.

511 Johnson, K. K., Bergin, M. H., Russell, A. G., and Hagler, G. S. W.: Field Test of Several Low-Cost Particulate Matter Sensors
512 in High and Low Concentration Urban Environments, *Aerosol Air Qual. Res.*, 18, 565–578,
513 <https://doi.org/10.4209/aaqr.2017.10.0418>, 2018.

514 Kelly, K. E., Whitaker, J., Petty, A., Widmer, C., Dybwad, A., Sleeth, D., Martin, R., and Butterfield, A.: Ambient and
515 laboratory evaluation of a low-cost particulate matter sensor, *Environ. Pollut.*, 221, 491–500,
516 <https://doi.org/10.1016/j.envpol.2016.12.039>, 2017.

517 Kim, K.-H., Kabir, E., and Kabir, S.: A review on the human health impact of airborne particulate matter, *Environ. Int.*, 74,
518 136–143, <https://doi.org/10.1016/j.envint.2014.10.005>, 2015.

519 Kloog, I., Nordio, F., Coull, B. A., and Schwartz, J.: Incorporating Local Land Use Regression And Satellite Aerosol Optical
520 Depth In A Hybrid Model Of Spatiotemporal PM_{2.5} Exposures In The Mid-Atlantic States, *Environ. Sci. Technol.*, 46, 11913–
521 11921, <https://doi.org/10.1021/es302673e>, 2012.

522 Kuula, J., Mäkelä, T., Aurela, M., Teinilä, K., Varjonen, S., González, Ó., and Timonen, H.: Laboratory evaluation of particle-
523 size selectivity of optical low-cost particulate matter sensors, *Atmospheric Meas. Tech.*, 13, 2413–2423,
524 <https://doi.org/10.5194/amt-13-2413-2020>, 2020.

525 Lee, H. J., Chatfield, R. B., and Strawa, A. W.: Enhancing the Applicability of Satellite Remote Sensing for PM_{2.5} Estimation
526 Using MODIS Deep Blue AOD and Land Use Regression in California, United States, *Environ. Sci. Technol.*, 50, 6546–6555,
527 <https://doi.org/10.1021/acs.est.6b01438>, 2016.

528 Liang, L.: Calibrating low-cost sensors for ambient air monitoring: Techniques, trends, and challenges, *Environ. Res.*, 197,
529 111163, <https://doi.org/10.1016/j.envres.2021.111163>, 2021.

530 Liu, H.-Y., Schneider, P., Haugen, R., and Vogt, M.: Performance Assessment of a Low-Cost PM_{2.5} Sensor for a near Four-
531 Month Period in Oslo, Norway, *Atmosphere*, 10, 41, <https://doi.org/10.3390/atmos10020041>, 2019.

532 Loh, B. G. and Choi, G. H.: Calibration of Portable Particulate Matter–Monitoring Device using Web Query and Machine
533 Learning, *Saf. Health Work*, 10, 452–460, <https://doi.org/10.1016/j.shaw.2019.08.002>, 2019.

534 Mccrowey, C., Sharac, T., Mangus, N., Jager, D., Brown, R., Garver, D., Wells, B., and Brittingham, H.: RAQSAPI: A Simple
535 Interface to the US EPA Air Quality System Data Mart API, 2022.

536 Miao, Y., Porter, W. C., Schwabe, K., and LeComte-Hinely, J.: Evaluating health outcome metrics and their connections to
537 air pollution and vulnerability in Southern California’s Coachella Valley, *Sci. Total Environ.*, 821, 153255,
538 <https://doi.org/10.1016/j.scitotenv.2022.153255>, 2022.

539 Miskell, G., Salmond, J., Alavi-Shoshtari, M., Bart, M., Ainslie, B., Grange, S., McKendry, I. G., Henshaw, G. S., and
540 Williams, D. E.: Data Verification Tools for Minimizing Management Costs of Dense Air-Quality Monitoring Networks,
541 *Environ. Sci. Technol.*, 50, 835–846, <https://doi.org/10.1021/acs.est.5b04421>, 2016.

542 Miskell, G., Salmond, J. A., and Williams, D. E.: Solution to the Problem of Calibration of Low-Cost Air Quality Measurement
543 Sensors in Networks, *ACS Sens.*, 3, 832–843, <https://doi.org/10.1021/acssensors.8b00074>, 2018.

544 Miskell, G., Alberti, K., Feenstra, B., Henshaw, G. S., Papapostolou, V., Patel, H., Polidori, A., Salmond, J. A., Weissert, L.,
545 and Williams, D. E.: Reliable data from low cost ozone sensors in a hierarchical network, *Atmos. Environ.*, 214, 116870,
546 <https://doi.org/10.1016/j.atmosenv.2019.116870>, 2019.

547 Morawska, L., Thai, P. K., Liu, X., Asumadu-Sakyi, A., Ayoko, G., Bartonova, A., Bedini, A., Chai, F., Christensen, B.,
548 Dunbabin, M., Gao, J., Hagler, G. S. W., Jayaratne, R., Kumar, P., Lau, A. K. H., Louie, P. K. K., Mazaheri, M., Ning, Z.,
549 Motta, N., Mullins, B., Rahman, M. M., Ristovski, Z., Shafiei, M., Tjondronegoro, D., Westerdahl, D., and Williams, R.:
550 Applications of low-cost sensing technologies for air quality monitoring and exposure assessment: How far have they gone?,
551 *Environ. Int.*, 116, 286–299, <https://doi.org/10.1016/j.envint.2018.04.018>, 2018.

552 Oroumiyeh, F., Jerrett, M., Del Rosario, I., Lipsitt, J., Liu, J., Paulson, S. E., Ritz, B., Schauer, J. J., Shafer, M. M., Shen, J.,
553 Weichenthal, S., Banerjee, S., and Zhu, Y.: Elemental composition of fine and coarse particles across the greater Los Angeles
554 area: Spatial variation and contributing sources, *Environ. Pollut.*, 292, 118356, <https://doi.org/10.1016/j.envpol.2021.118356>,
555 2022.

556 Ostro, B. D., Broadwin, R., and Lipsett, M. J.: Coarse and fine particles and daily mortality in the Coachella Valley, California:
557 a follow-up study, *J. Expo. Sci. Environ. Epidemiol.*, 10, 412–419, <https://doi.org/10.1038/sj.jea.7500094>, 2000.

558 Ouimette, J. R., Malm, W. C., Schichtel, B. A., Sheridan, P. J., Andrews, E., Ogren, J. A., and Arnott, W. P.: Evaluating the
559 PurpleAir monitor as an aerosol light scattering instrument, *Atmospheric Meas. Tech.*, 15, 655–676,
560 <https://doi.org/10.5194/amt-15-655-2022>, 2022.

561 Pinto, J. P., Lefohn, A. S., and Shadwick, D. S.: Spatial Variability of PM_{2.5} in Urban Areas in the United States, *J. Air Waste
562 Manag. Assoc.*, 54, 440–449, <https://doi.org/10.1080/10473289.2004.10470919>, 2004.

563 Pope, C. A. 3rd and Dockery, D. W.: Acute health effects of PM₁₀ pollution on symptomatic and asymptomatic children.,
564 *Am. Rev. Respir. Dis.*, 145, 1123–1128, <https://doi.org/10.1164/ajrccm/145.5.1123>, 1992.

565 Pope Iii, C. A.: Lung Cancer, Cardiopulmonary Mortality, and Long-term Exposure to Fine Particulate Air Pollution, *JAMA*,
566 287, 1132, <https://doi.org/10.1001/jama.287.9.1132>, 2002.

567 Qin, X., Pratt, K. A., Shields, L. G., Toner, S. M., and Prather, K. A.: Seasonal comparisons of single-particle chemical mixing
568 state in Riverside, CA, *Atmos. Environ.*, 59, 587–596, <https://doi.org/10.1016/j.atmosenv.2012.05.032>, 2012.

569 Rai, P. K.: Impacts of particulate matter pollution on plants: Implications for environmental biomonitoring, *Ecotoxicol.
570 Environ. Saf.*, 129, 120–136, <https://doi.org/10.1016/j.ecoenv.2016.03.012>, 2016.

571 Sardar, S. B.: Seasonal and spatial variability of the size-resolved chemical composition of particulate matter (PM₁₀) in the
572 Los Angeles Basin, *J. Geophys. Res.*, 110, D07S08, <https://doi.org/10.1029/2004JD004627>, 2005.

573 Slowikowski, K., Schep, A., Hughes, S., Dang, T. K., Lukauskas, S., Irisson, J.-O., Kamvar, Z. N., Ryan, T., Christophe, D.,
574 Hiroaki, Y., Gramme, P., Abdol, A. M., Barrett, M., Cannoodt, R., Krassowski, M., Chirico, M., and Aphalo, P.: ggrepel:
575 Automatically Position Non-Overlapping Text Labels with “ggplot2,” 2022.

576 Snyder, E. G., Watkins, T. H., Solomon, P. A., Thoma, E. D., Williams, R. W., Hagler, G. S. W., Shelow, D., Hindin, D. A.,
577 Kilaru, V. J., and Preuss, P. W.: The Changing Paradigm of Air Pollution Monitoring, *Environ. Sci. Technol.*, 47, 11369–
578 11377, <https://doi.org/10.1021/es4022602>, 2013.

579 Spinu, V., Grolemond, G., Wickham, H., Vaughan, D., Lyttle, I., Costigan, I., Law, J., Mitarotonda, D., Larmarange, J., Boiser,
580 J., and Lee, C. H.: lubridate: Make Dealing with Dates a Little Easier, 2022.

581 Weissert, L., Miles, E., Miskell, G., Alberti, K., Feenstra, B., Henshaw, G. S., Papapostolou, V., Patel, H., Polidori, A.,
582 Salmond, J. A., and Williams, D. E.: Hierarchical network design for nitrogen dioxide measurement in urban environments,
583 *Atmos. Environ.*, 228, 117428, <https://doi.org/10.1016/j.atmosenv.2020.117428>, 2020.

584 Wickham, H. and RStudio: tidyverse: Easily Install and Load the “Tidyverse,” 2022.

585 Wickham, H., François, R., Henry, L., Müller, K., and RStudio: dplyr: A Grammar of Data Manipulation, 2022a.

586 Wickham, H., Chang, W., Henry, L., Pedersen, T. L., Takahashi, K., Wilke, C., Woo, K., Yutani, H., Dunnington, D., and
587 RStudio: ggplot2: Create Elegant Data Visualisations Using the Grammar of Graphics, 2022b.

588 Witiw, M. R. and LaDochy, S.: Trends in fog frequencies in the Los Angeles Basin, *Atmospheric Res.*, 87, 293–300,
589 <https://doi.org/10.1016/j.atmosres.2007.11.010>, 2008.

590 Zeileis, A., Grothendieck, G., Ryan, J. A., Ulrich, J. M., and Andrews, F.: zoo: S3 Infrastructure for Regular and Irregular
591 Time Series (Z's Ordered Observations), 2022.

592 Zheng, T., Bergin, M. H., Johnson, K. K., Tripathi, S. N., Shirodkar, S., Landis, M. S., Sutaria, R., and Carlson, D. E.: Field
593 evaluation of low-cost particulate matter sensors in high and low concentration environments, *Aerosols/In Situ*
594 *Measurement/Instruments and Platforms*, <https://doi.org/10.5194/amt-2018-111>, 2018.

595 Zimmerman, N.: Tutorial: Guidelines for implementing low-cost sensor networks for aerosol monitoring, *J. Aerosol Sci.*, 159,
596 105872, <https://doi.org/10.1016/j.jaerosci.2021.105872>, 2022.

597

598